Hindawi
Mathematical Problems in Engineering
Volume 2019, Article ID 2720873, 9 pages
https://doi.org/10.1155/2019/2720873

Research Article

Simulation Analysis of Bionic Robot Fish Based on MFC Materials

Chengguang Zhang

School of Mechanical and Electrical Engineering, Zhoukou Normal University, Zhoukou 466001, Henan, China

Correspondence should be addressed to Chengguang Zhang; zhangchengguang@126.com

Received 17 February 2019; Accepted 9 May 2019; Published 4 June 2019

Academic Editor: Giovanni Garcea

With the development of marine resources, research on underwater robots has received unprecedented attention. The discovery and application of new smart materials provide new ideas for the research of underwater robots, which can overcome the issues of traditional underwater robots and optimize their design. A macro fiber composite (MFC) is a new type of piezoelectric fiber composite that combines actuators and sensors. The material has excellent deflection, good flexibility, and a high electromechanical coupling coefficient. Bionic mechatronics design is an effective way to innovate mechatronics in the future and can significantly improve mechatronics system performance. As an important issue for the design of bionic mechatronics, it is necessary to make robots as soft as natural organisms to achieve similar biological movement with both higher efficiency and performance. Compared with traditional rigid robots, the design and control of a soft robotic fish are difficult because the coupling between the flexible structure and the surrounding environment should be considered, which is difficult to solve due to the large deformation and coupling dynamics. In this paper, an MFC smart material is applied as an actuator in the design of bionic robotic fish. Combined with the piezoelectric constitutive and elastic constitutive equations of the MFC material, the voltage-drive signal is converted to a mechanical load applied to the MFC actuator, which makes the MFC material deform and drives the movement of the robotic fish. The characteristics of caudal fin motion during the swimming process of the bionic robotic fish were analyzed by an acoustic-solid coupling analysis method. The motion control analysis of the bionic robotic fish was carried out by changing the applied driving signal. Through numerical analysis, a new type of soft robotic fish was designed, and the feasibility of using an MFC smart material for underwater bionic robotic fish actuators was verified. The new soft robotic fish was successfully developed to achieve high performance.

1. Introduction

The fish propulsion model, which has been selected by nature, is by far the most efficient and adaptable to the underwater environment. Therefore, research on new bionic robotic fish has become a hot topic in the field of underwater robotic research.

In general, the propulsion structure of an oscillating propulsion fish is mostly the caudal fin, which is suitable for long-distance and long-term sustainable swimming (cruising), and its propulsion efficiency is higher than that of the fish with fluctuating body propulsion [1–4]. Fish with fluctuating body propulsion have higher flexibility and are able to adapt to subtle and complex environmental changes.

According to the different driving modes, the research of bionic robotic fish is divided into two categories: one category is a bionic robotic fish driven by conventional drives such as a hydraulic motor or a servo motor, and the other category is a bionic robot powered by new smart materials with special drive elements, such as shape memory alloys (SMAs) and piezoelectric ceramics (e.g., lead zirconate titanate, PZT).

Because of issues including large volume, considerable noise, and poor flexibility in the traditional drive mode of robotic fish, scholars in the field of underwater robotic research have begun to change their focus to small, fast, and flexible robotic fish. With the development of smart materials, this function is increasingly more powerful. Many scholars have applied smart materials that function like fish muscle tissue to the design of bionic robotic fish, providing power as an actuator [5–9]. Thus, the power of bionic robotic fish is simplified, and the volume of robotic fish is reduced, with more flexible structures and movement.

Because of their fish-like streamline shape, bionic robotic fish have a fluid resistance device that is smaller than the propeller device during propulsion. The noise of the bionic robotic fish is less than that of propeller devices, which is difficult to detect and identify by sonar. Bionic robotic fish can save a great deal of energy with improved efficiency while swimming. Bionic robotic fish integrate the propulsion system with the control capability.

2. Research on Piezoelectric Smart Composites

2.1. Introduction to Piezoelectric Composites. Piezoelectric fiber composites are composed of piezoelectric fibers and resin substrates by means of specific ratios, spatial distributions, and connections between them, combining the advantages of traditional piezoelectric polymers with resin substrates [10]. Because of the protective effect of the resin substrates, piezoelectric fiber composites have considerably improved strength and toughness compared with traditional piezoelectric polymers. At the same time, the composites change the ratio and spatial distribution of the resin substrate, which greatly improves the flexibility and piezoelectric properties of the composites [11].

The piezoelectric fiber of the macro fiber composite (MFC) material is laid in the direction of the working surface, polarized along the length of the fiber, and arranged by interdigitated electrodes [12]. This special electrode arrangement allows the driver to make greater use of the applied electric field to achieve the best inverse piezoelectric effects. Driven by the same external electric field, the maximum mechanical response is generated and, thus, a greater driving force and displacement are obtained.

Because MFCs have advantages of light weight and high efficiency, are easy to manufacture, and are suitable for surface structures, their research and application are more in-depth and extensive, especially in the field of active control.

In this experiment, the MFC smart piezoelectric actuator was selected as the driving unit of the bionic robotic fish. The external voltage was used to control the deformation of the MFC actuator, and the propulsion mode of the caudal fin swing was realized. The M-8528-P1 smart material, produced by Smart Materials Corp., was selected and is shown in Figure 1 and Table 1.

2.2. Piezoelectric Constitutive Equation of MFC Materials. The piezoelectric equation is established on the basis of thermodynamic equations, which are the *d*-type and *e*-type piezoelectric equations, and the independent variable is electric field strength E_v.

$$\begin{bmatrix} D \\ \varepsilon \end{bmatrix} = \begin{bmatrix} r^T & d \\ d & s^E \end{bmatrix} \begin{bmatrix} E_v \\ \sigma \end{bmatrix} \tag{1}$$

$$\begin{bmatrix} D \\ \sigma \end{bmatrix} = \begin{bmatrix} r^S & e \\ -e & c^E \end{bmatrix} \begin{bmatrix} E_v \\ \varepsilon \end{bmatrix} \tag{2}$$

where D, σ, E_v, and ε are electrical displacement, mechanical stress, electric field strength, and total strain vector, respectively; r^T and r^S are the pressure dielectric constant and the pressure strain constant, respectively; d is the piezoelectric strain constant matrix; e is the piezoelectric pressure constant matrix; and s and c are the flexibility coefficient matrix and stiffness coefficient matrix of the material, respectively. The superscripts T and S indicate that the pressure is constant or the strain is constant, and the superscript E indicates that the external applied electric field strength is constant.

The strain of the piezoelectric material can be decomposed into elastic strain and piezoelectric strain, and the vector form is as follows.

$$\varepsilon = \varepsilon^X + \varepsilon^E \tag{3}$$

where ε^X and ε^E represent the elastic strain and piezoelectric strain, respectively, of the piezoelectric material, which can be obtained by the piezoelectric constitutive equation.

$$\varepsilon = d_t E_V + s^E X \tag{4}$$

It can be obtained by (3) and (4).

$$\begin{aligned} \varepsilon^X &= s^E X, \\ \varepsilon^E &= d_t E_V \end{aligned} \tag{5}$$

From formula (4), it can be seen that the mechanical analysis of piezoelectric materials has one more piezoelectric strain term than the conventional elastic material. This piezoelectric strain can be replaced by a mechanical load so that the piezoelectric material can be considered a conventional material to analyze the corresponding stress [14].

$$\sigma_c = c^E \varepsilon^E = c^E d_t E_V \tag{6}$$

The stress is converted into a load

$$F = \int_{A_{area}} \sigma_c dA = \int_{A_{area}} c^E d_t E_V dA \tag{7}$$

where A is the area of the piezoelectric unit.

In the case of small deformation, the stress-strain relationship of the MFC is only generated by the external forces, which conforms to the constitutive relationship of elastic materials, that is, the mechanical response of piezoelectric fiber composites [15]. When the piezoelectric fiber is subjected to external forces and produces a positive piezoelectric effect, the positive and negative charge will be concentrated on different surfaces of the piezoelectric fibers, thereby generating an electrical displacement inside the MFC. When an external electric field is applied to the piezoelectric fiber to produce an inverse piezoelectric effect, the movement of the internal positive and negative charge will also produce an electrical displacement.

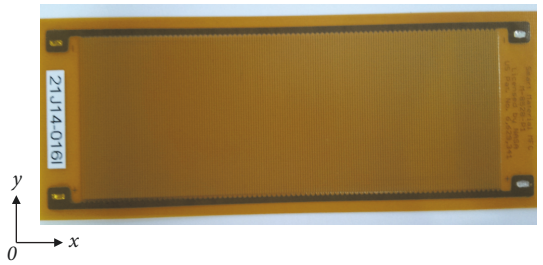

Figure 1: M-8528-P1 smart material.

Table 1: Properties of the MFC material parameters [13].

Item	Symbol	Specification
Tensile modulus (GPa)	E_1	30.336
	E_1	15.9
Poisson's ratio	v_{12}	0.31
	v_{12}	0.16
Shear modulus (GPa)	G	5.515
Piezoelectric constants (low electric field) (pm/V)	d_3	400
	d_{31}	-170
Piezoelectric constants (high electric field) (pm/V)	d_{33}	460
	d_{31}	-210

The x-y plane of piezoelectric fiber composites is isotropic, which is equivalent to a transverse isotropic material. At the same time, piezoelectric fibers are polarized along the z-axis direction.

$$\begin{bmatrix} \sigma_x \\ \sigma_y \\ \sigma_z \\ \sigma_{yz} \\ \sigma_{zx} \\ \sigma_{xy} \end{bmatrix} = \begin{bmatrix} c_{11} & c_{12} & c_{13} & 0 & 0 & 0 \\ c_{21} & c_{22} & c_{23} & 0 & 0 & 0 \\ c_{31} & c_{32} & c_{33} & 0 & 0 & 0 \\ 0 & 0 & 0 & c_{44} & 0 & 0 \\ 0 & 0 & 0 & 0 & c_{55} & 0 \\ 0 & 0 & 0 & 0 & 0 & c_{66} \end{bmatrix} \begin{bmatrix} \varepsilon_x \\ \varepsilon_y \\ \varepsilon_z \\ \gamma_{yz} \\ \gamma_{zx} \\ \gamma_{xy} \end{bmatrix} \tag{8}$$

where $c_{11} = c_{22}$, $c_{12} = c_{21}$, $c_{13} = c_{31} = c_{23} = c_{32}$, and $c_{44} = 2(c_{11} - c_{12})$.

By comparing the above stress methods, the expression of the piezoelectric driving stress can be rewritten as

$$\sigma_x = \frac{c_{11}c_{33} - c_{13}c_{31}}{c_{33}} d_{33}E_V + \frac{c_{12}c_{33} - c_{13}c_{32}}{c_{33}} d_{31}E_V \tag{9}$$

$$\sigma_y = \frac{c_{21}c_{33} - c_{23}c_{31}}{c_{33}} d_{33}E_V + \frac{c_{22}c_{33} - c_{23}c_{32}}{c_{33}} d_{31}E_V \tag{10}$$

$$\begin{aligned} \begin{bmatrix} L_x \\ L_y \end{bmatrix} &= \frac{1}{2} \begin{bmatrix} \sigma_x \\ \sigma_y \end{bmatrix} \\ &= \frac{1}{2\left(1 - v_{xy}v_{yx}\right)} \begin{bmatrix} E_x & E_x v_{yx} \\ E_y v_{xy} & E_y \end{bmatrix} \begin{bmatrix} d_{33} \\ d_{31} \end{bmatrix} \frac{V}{W_{pitch}} \end{aligned} \tag{11}$$

where W_{pitch} is the electrode spacing.

Because of the inverse piezoelectric effect, the MFC can produce a large axial force and bending moment to make the structure deformation. For the bionic robotic fish of the body and/or caudal fin (BCF) propulsion mode, the bending deformation produced by the MFC material can simulate the swinging state of the caudal fin structure [16].

3. Acoustic-Solid Coupling Analysis

The modal analysis of solid structures can help predict the structural vibration and modal frequency of the structure and has an important reference significance for the design and performance of the structure. However, modal analysis does not take into account the influence of the working environment when calculating the natural modes. The same structure works in different environments, and its modal properties and even other important dynamic properties are significantly different. The working environment for bionic robotic fish is a fluid. The dry modal analysis that does not consider the effects of fluids can only be used as a reference. The wet mode containing the fluid environment is the real mechanical characteristic under its working state.

The influence of a fluid on the inherent characteristics of the structure is mainly manifested in two aspects: one is the prestressing effect caused by the pressure load acting on the surface of the structure, and the other is the additional mass effect caused by the vibration of the fluid along with the structure [17, 18]. To obtain accurate dynamics of the structure working in a fluid working environment, the effects of the above two factors must be considered.

For the acoustic-solid coupling model of the bionic robotic fish, the effect of prestressing effects need not be

considered. The effect of the prestressing effect is that the flow field pressure acts on the structure to cause a deformation of the structure, and the internal stress of the structure is produced before the external load is applied. The bionic robotic fish model is in the flow field. In the static state, the macroscopic force of the surrounding flow field is zero, and the transverse is symmetrical. Therefore, the robotic fish does not produce a deformation and does not need to consider the prestressing effect.

The main idea of using the acoustic-solid coupling algorithm to address the fluid-solid coupling problem is to regard the space area occupied by fluids as the acoustic field area. The acoustic unit is used to simulate the fluid, and the finite element equation of the acoustic space is listed [19] and then combined with the finite element equation of the structural to solve it. The finite element equation for acoustic-solid coupling analysis is shown as follows.

$$\begin{bmatrix} M_a & P_a A \\ 0 & M_S \end{bmatrix} \begin{bmatrix} P \\ \ddot{U} \end{bmatrix} + \begin{bmatrix} C_a \\ 0 \end{bmatrix} \begin{bmatrix} P \\ \dot{U} \end{bmatrix} + \begin{bmatrix} K_a & 0 \\ 0 & K_S \end{bmatrix} \begin{bmatrix} P \\ U \end{bmatrix} = \begin{bmatrix} 0 \\ F_S \end{bmatrix} \tag{12}$$

where M_a, C_a, K_a, *and* A are the overall mass matrix, damping matrix, stiffness matrix, and coupling matrix of the acoustic unit, respectively; and M_s, C_s, *and* K_s are the overall mass matrix, damping matrix, and stiffness matrix of the structure, respectively.

4. Bionic Robotic Fish and Finite Element Model

4.1. Bionic Robotic Fish Design. The bionic robotic fish consisted of two MFC plates sandwiched with a carbon fiber reinforced polymer (CFRP) substrate, in which the MFC was symmetrically distributed. A sinusoidal drive signal with the same frequency and opposite phase was applied. When a piece of the MFC shrinks and another piece of MFC stretches, the middle of the CFRP substrate produced a periodic bending deformation.

The finite element method was used to simulate and analyze the acoustic coupling problem using ANSYS software. The acoustic elements consisted of 4 degrees of freedom: three for the optional displacement and one for the pressure to achieve the desired fluid-structure coupling. A consistent matrix coupling was established between the structural and fluid elements.

In addition, a weight was added to the head of the robotic fish to limit the lateral displacement of the head, which can increase the lateral deformation of the tail of the robotic fish, enhance the effect of pushing the water flow, and increase the propulsive force. The function was the same as that of a cantilever beam structure [20, 21].

The MFC material was of an M-8528-P1 type. The thickness of the central CFRP plate was 0.2 mm. The head weight was 2.5 mm diameter cylindrical structural steel with a density of 7850 kg/m^3. The structural parameters of the remaining bionic robotic fish are shown in Table 2.

Table 2: Structural parameters of the bionic fish model.

Item	Specification
Body length (mm)	167
Maximum height of the body (mm)	55
Caudal fin height (mm)	50
Body thickness (mm)	CFRP 0.2
Actuator type	M-8528-P1
Actuator size (mm)	112 × 40
Actuator active area size (mm)	85 × 28

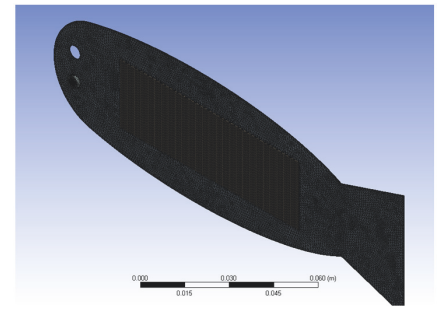

Figure 2: Geometric model of the bionic robotic fish.

4.2. Finite Element Model of Bionic Robotic Fish. To simulate the vibration performance of a real fluid, a spherical computing domain with a diameter of 200 mm was used, and the robotic fish was located in the center, as shown in Figures 2 and 3, and its finite element model is shown in Figure 4. In addition, due to the high-voltage driving characteristics of the MFC material, the fluid environment in the experiment was selected as the insulated perfluorinated liquid FC-3283 to ensure that the fluid remained stable, with no dissipation during the experiment.

4.3. Modal Analysis of Bionic Robotic Fish. To predict the vibration pattern and modal frequency of the bending deformation, a modal analysis of the acoustic-solid coupling model of the bionic robotic fish and the flow field is required. The finite element equation of the structure is as follows [22].

$$M_S\ddot{U} + K_S U = F_S + f_F \tag{13}$$

$$f_F = RP = \int_{SF} N_S{}^T n N_F P dS \tag{14}$$

where M_S and K_S are the structural matrix and stiffness matrix, respectively; U is the displacement; F_S is the external force of the structure; f_F is the pressure vector describing the acoustic-solid coupling; P is the fluid pressure; R is an effective area matrix that represents the interface between the robotic fish structure and the fluid junction with each node; N_S and N_F represent the finite element function of the fish structure and fluid structure, respectively; and n is the fluid boundary vector.

Table 3: Acoustic-solid coupled modal frequency.

Item	Modal Frequency (Hz)		
Bionic robotic fish in the air	41.50	66.06	83.03
Bionic robotic fish in the flow field	6.13	16.47	29.70

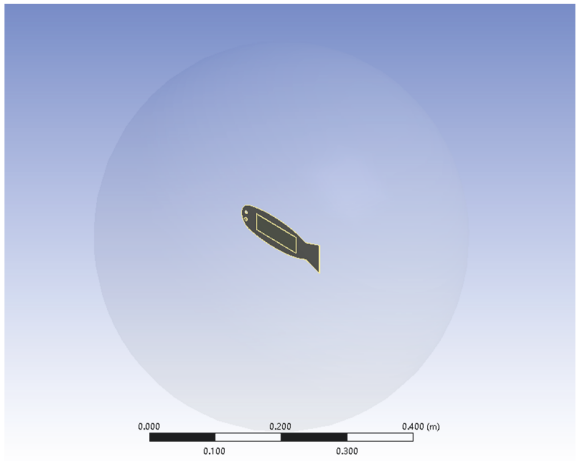

Figure 3: Acoustic-solid coupling calculation domain.

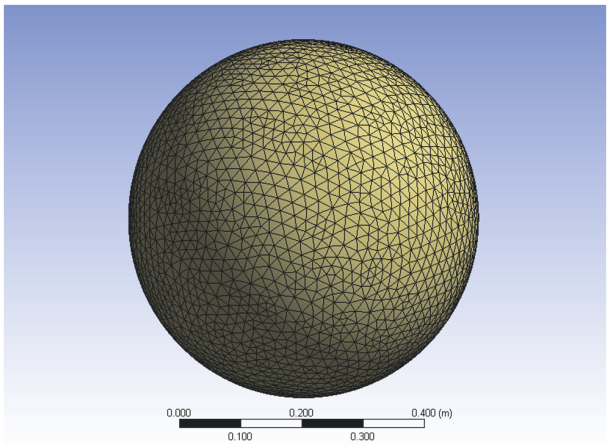

Figure 4: Finite element model of the flow field.

The fluid-related finite element equations are shown as follows.

$$M_F\ddot{P} + K_F P = F_F + f_S \tag{15}$$

$$f_S = -\rho_f R^T \ddot{U} \tag{16}$$

where M_F and K_F represent the mass matrix and the stiffness matrix, respectively; P is the fluid pressure; F_F is the added item of the mass; and ρ_f is the static density of the fluid.

The coupling between the structure and the flow field is described by the boundary pressure. The deformation of the structure is affected by the fluid pressure, and the displacement change in the structure is transmitted to the fluid domain. Finally, the effect of simulating fluid-solid coupling is achieved.

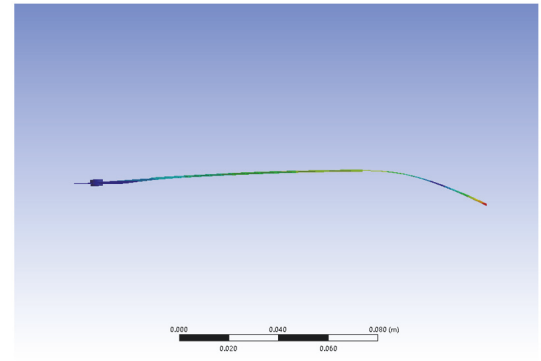

Figure 5: Modal analysis of the acoustic-solid coupling method.

From the analysis results in Table 3, it can be seen that the modal frequency of the robotic fish in the flow field is obviously lower than the modal frequency in the air. Additionally, the higher the modal order is, the greater the frequency difference is. This difference is mainly due to the existence of the static pressure of the fluid resulting in extra mass additions to the structure, which results in a decrease in the corresponding modal frequency.

The corresponding vibration mode of the acoustic-solid coupling modal analysis is shown in Figure 5. Among them, the first-order and second-order bending deformations occur at 6.13 Hz and 29.70 Hz, respectively.

Considering the first-order bending mode, the maximum displacement of the whole robotic fish structure appears at the tail of the caudal fin. There is almost no displacement in the z-axis direction at the junction of the caudal fin and the body, and the displacement is basically caused by the caudal fin. The rear 1/3 part of the robotic fish swings to produce propulsion. The lateral amplitude of the first 2/3 part is small, and the main function is to maintain the balance of the robotic fish.

5. Transient Analysis of Bionic Robotic Fish

Transient dynamics analysis is a time domain analysis. That is, the applied load changes with time, and the dynamic response of the structure to the time-varying load is analyzed. Transient dynamics analysis is widely used and is typically used to simulate the stiffness and strength of the structural dynamic response.

Transient dynamics analysis includes linear transient dynamics analysis and nonlinear transient dynamics analysis. Linear transient dynamics analysis means that no nonlinear behavior is included in the model, which is suitable for

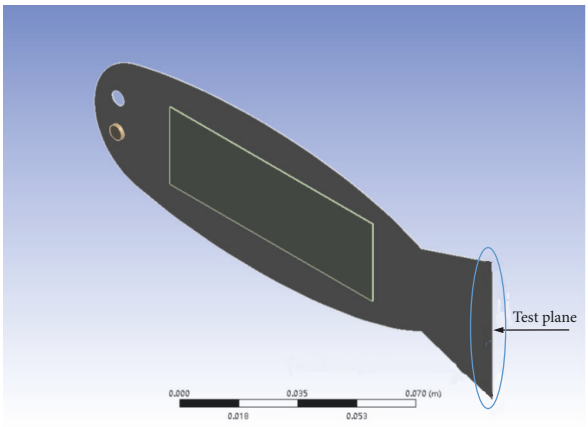

Figure 6: Transient analysis test plane.

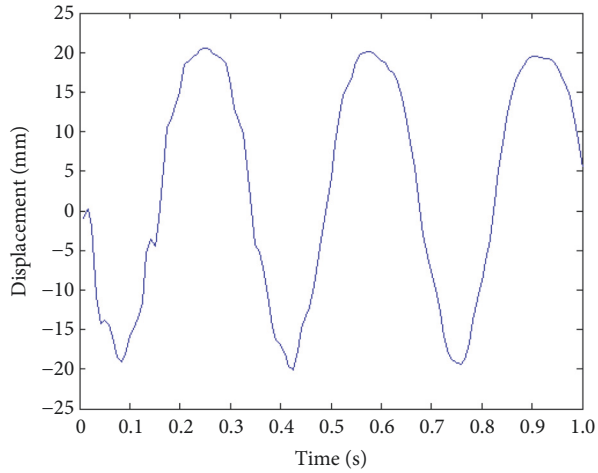

Figure 7: Swing amplitude of the caudal fin (straight line).

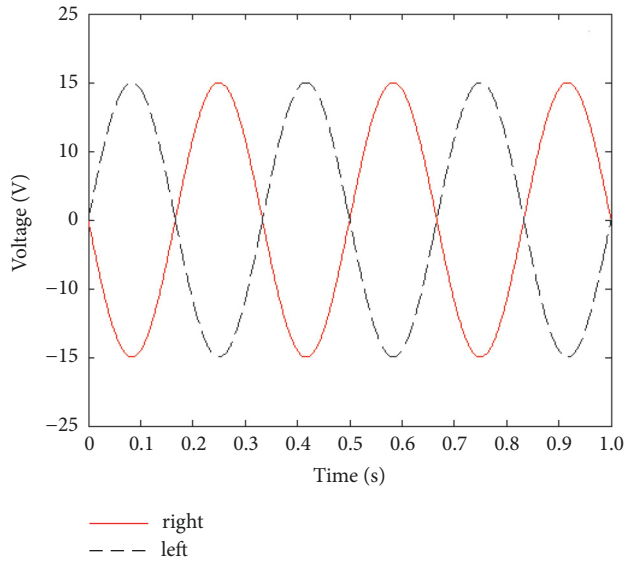

Figure 8: Drive signal (straight line).

structural models with linear, small displacements and small strains and a constant total stiffness of the material properties. Nonlinear transient dynamics analysis considers a variety of nonlinear behaviors, including the nonlinear properties of materials, large deformations, large displacements, contacts, and collisions. Because the MFC smart material itself is nonlinear, there are nonlinear effects in the bionic robotic fish, such as large deformations, and the influence of nonlinear factors needs to be taken into account in the transient analysis [23, 24].

The coupled transient analysis was used to identify the dynamic behavior of the soft robotic fish in fluid. The robotic fish structural domain was described by three-dimensional (3D) SOLID 186 elements, and 3D FLUID 30 elements were used to simulate the fluid domain and coupled interface.

The results of modal analysis show that the process of robotic fish propulsion is mainly in the state of the first-order mode, so the driving frequency applied in the experiment is approximately 6 Hz. After a comparison of the simulations, we found that the robotic fish had better motion and response when the load frequency was 3 Hz. Therefore, the final drive signal is a sinusoidal signal with an amplitude of -500 V~1500 V and a frequency of 3 Hz. Under this signal, the terminal plane of the caudal fin is used as the test plane, as shown in Figure 6.

As shown in Figure 7, the displacement of the caudal fin end in a period is close to a sine wave with time, and the oscillation period is the same as the driving signal, which proves that the MFC material has strong real-time driving. The swing peak of the test plane is close to 40 mm, which is approximately 1/4 of the overall length of the robotic fish and slightly smaller than a natural fish propelled by the tuna model.

6. Motion Control Analysis of Bionic Robotic Fish

To realize the complete motion posture of the bionic robotic fish, the acoustic-solid coupling method is used to simulate the steering motion of the robotic fish.

Changing the drive signal frequency can change the deformation of the MFC material. This change can facilitate the different deformations of the MFC materials on both sides in a cycle and complete the steering. However, observational studies of an actual fish have shown that the oscillation frequency of the caudal fin is almost identical, and whether the fish is swimming straight or turning, there is no obvious frequency change. Instead, the neutral surface of the fish is shifted to the left or right through the shrinkage of the muscles on both sides, and then the caudal fin swing propulsion is completed near the neutral surface [25]. In contrast, in the design of the bionic robotic fish, through a change in the driving voltage amplitude of the MFC material on both sides, different degrees of shrinkage of the muscles on both sides can be simulated to realize the offset of the neutral surface.

When the bionic robotic fish moves forward, the driving signals on both sides have the same amplitude and opposite

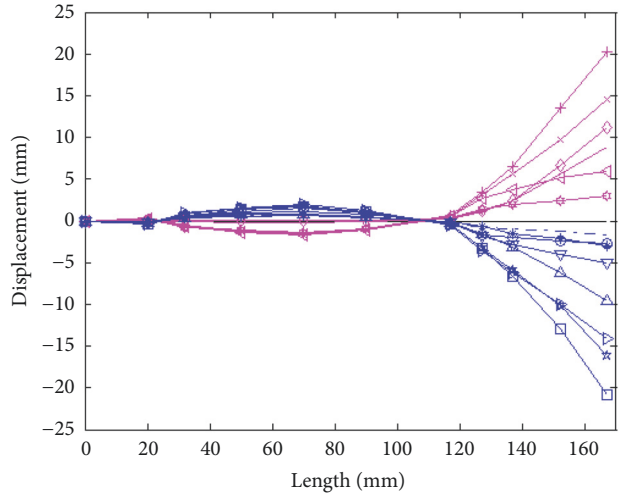

Figure 9: Bionic robotic fish, straightforward.

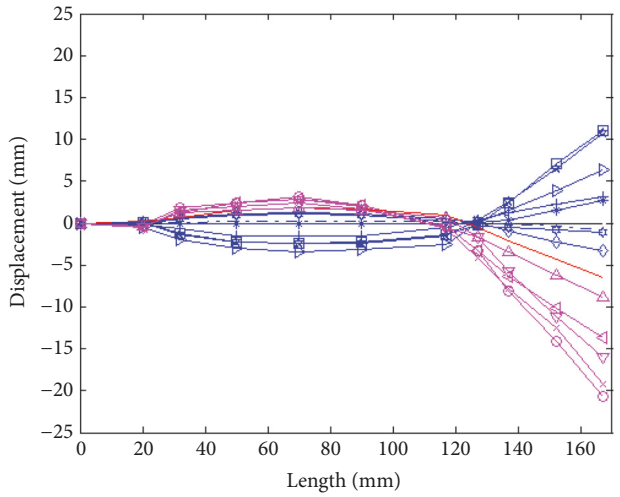

Figure 11: Bionic robotic fish, left turn.

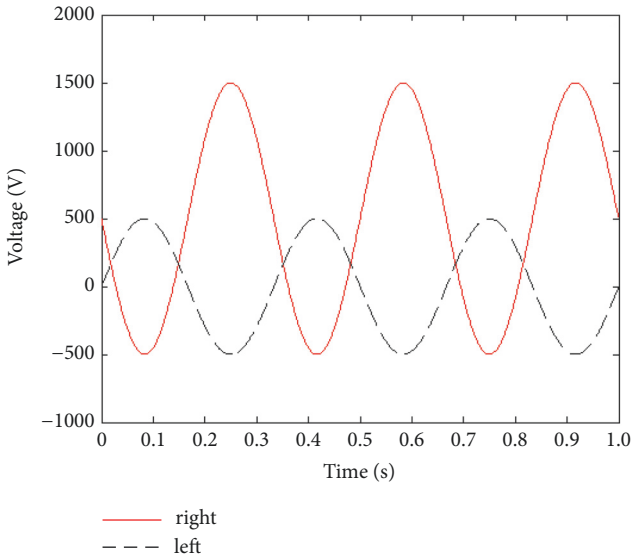

Figure 10: Drive signal (turn left).

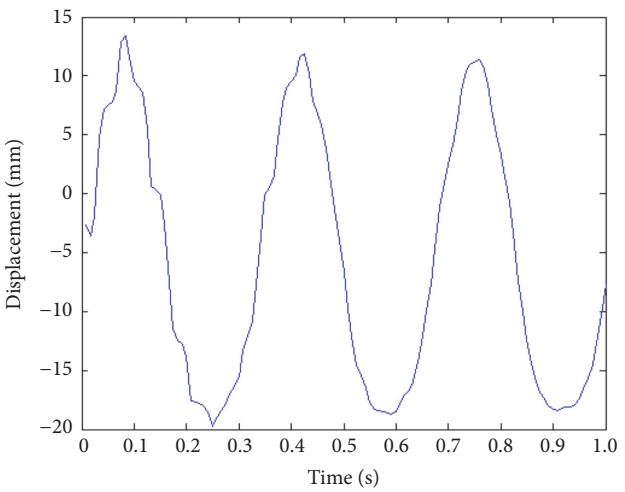

Figure 12: The swing amplitude of the caudal fin (turn left).

phases, as shown in Figure 8. Using a sinusoidal signal with a frequency of 3 Hz as the driving signal, the amplitudes of the driving signals on the left and right sides are changed, and the signals on both sides have an opposite phase [26]. The bionic robotic fish motion posture is shown in Figure 9, and the caudal fin at the end of the swing peak is approximately 40 mm. The propulsion force obtained by the robotic fish swinging through the caudal fin makes it move forward.

The change in the drive signal of the MFC drive is shown in Figure 10, reducing the positive phase amplitude of the left drive signal while keeping the right inverse phase amplitude unchanged. The effect of such a drive signal is that the shrinkage effect of the two MFC drives is the same, while the stretching of the left MFC actuator is less than that of the right actuator. The balance point of the CFRP substrate is shifted to the left side, so that the neutral surface is offset to the left side, and the left turn is completed.

As shown in Figure 11, the neutral surface of the bionic robotic fish is shifted to the left, so that the balance position of the caudal fin swing is changed, and the action of turning left is completed. It is also possible to control the steering radius of the robotic fish by controlling the amplitude difference of the drive signal on both sides, and if the amplitude difference is larger, the steering radius is smaller.

Figure 12 shows the z-axis displacement of the caudal fin test plane after applying an asymmetric voltage signal on both sides of the MFC driver. As seen from the figure, the caudal fin swings in a sinusoidal form, and the frequency is maintained at 3 Hz, which is the same as the drive signal frequency. However, the difference from the forward motion is the sinusoidal signal formed by the caudal fin oscillation, where the positive amplitude decreases and the inverse amplitude increases; that is, the amplitude in the negative direction of the z-axis increases by approximately 3 mm.

The action of the bionic robotic fish steering is the same as that of an actual fish when turning, and the equilibrium

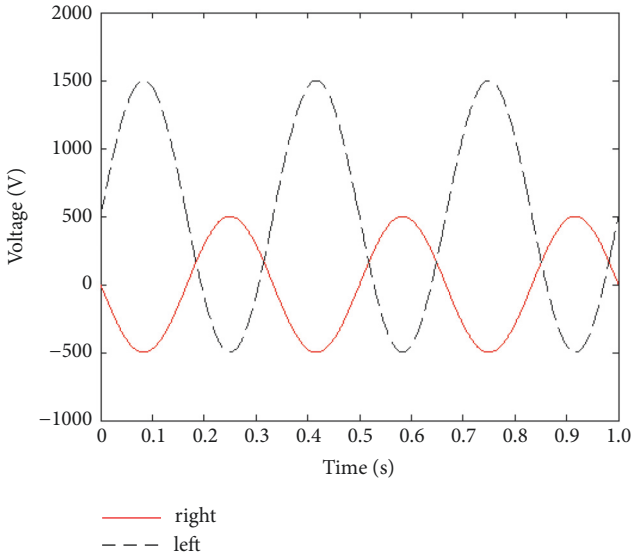

Figure 13: Drive signal (right turn).

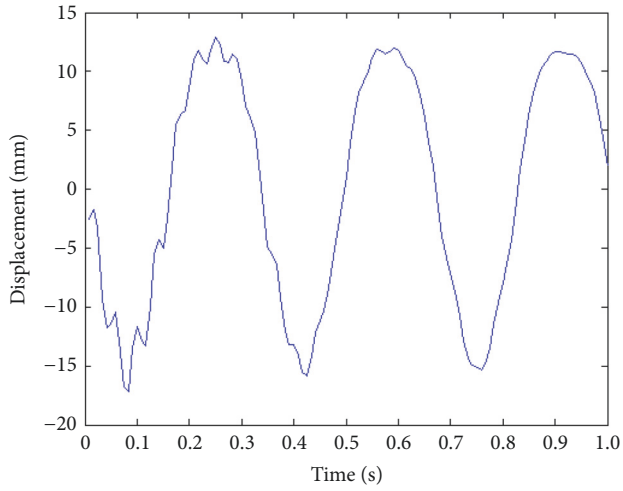

Figure 15: Swing amplitude of the caudal fin (right turn).

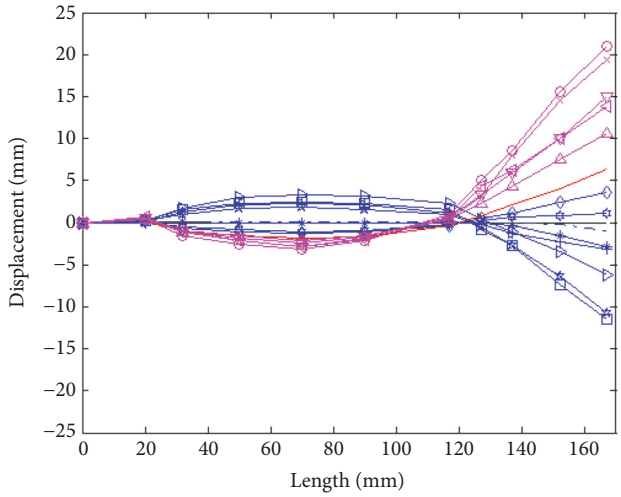

Figure 14: Bionic robotic fish turning right.

position of the caudal fin swing is changed by the static shrink degree of the muscles on both sides. The greater the difference in the muscle shrinkage between the two sides is, the greater the offset of the equilibrium position relative to the axis of the fish is, and the smaller the turning radius is. The caudal fin of the fish remains in the vicinity of the new equilibrium position with the same amplitude and period of oscillation, completing the entire steering action. For the bionic robotic fish, the equilibrium point of the caudal fin swing is offset to the left side by approximately 3 mm (negative direction of the z-axis). The caudal fin of the bionic robotic fish maintains the same frequency of oscillation near the new equilibrium position, achieving a steering propulsion.

Similarly, when the robotic fish turns right, the driving signal, the propulsion mode, and the caudal fin test plane oscillating waveform are represented by Figures 13, 14, and 15, respectively. To achieve the right movement of the robotic fish, the amplitude of the right drive signal should be reduced so that the stretch deformation of the right MFC is smaller than that of the left MFC and the shrinkage state of the MFC on both sides of the same deformation. The neutral surface of the robotic fish is offset to the right, and the caudal fin swings near the right side of the neutral surface to complete the right turn action.

The amplitude and DC offset of the MFC driving signals on the left and right sides are changed to simulate the true contraction of the muscles on both sides of the fish to achieve the turning action of the bionic robotic fish. The turning radius is related to the difference between the amplitudes of the signals on both sides. The larger the difference between the amplitudes is, the smaller the turning radius is, and the faster the turning action is.

7. Conclusion

The finite element model of the bionic robotic fish based on MFC material was established. The acoustic unit was used to simulate the discretized fluid calculation domain, and the additional mass effect of bionic robotic fish in the fluid working environment was considered. The modal frequency and vibration pattern of the robotic fish moving in the fluid were obtained by wet modal analysis, and the dynamic characteristics of the robotic fish structure under working conditions were obtained. The propulsion action of the bionic robotic fish driven by a sinusoidal voltage in the fluid calculation domain was simulated.

On the basis of the forward movement of the bionic robotic fish, the amplitude and phase difference of the MFC driving signals on the left and right sides were changed, and the degree of shrinkage of the muscles on both sides was simulated to realize the steering action of the bionic robotic fish.

Data Availability

The data used to support the findings of this study are included within the article.

Conflicts of Interest

The author declares that there are no conflicts of interest regarding the publication of this paper.

Acknowledgments

This work was supported by the National Natural Science Foundation of China (Grant no. 51275116) and Natural Science Foundation of Henan, China (Grant no. 182300410250).

References

[1] E. Kim and Y. Youm, "Design and dynamic analysis of fish robot: Potuna," in *Proceedings of the IEEE International Conference on Robotics and Automation*, vol. 5, pp. 4887–4892, 2004.

[2] P. W. Webb, "Form and Function in Fish Swimming," *Scientific American*, vol. 251, pp. 72–83, 1984.

[3] K. H. Low, C. W. Chong, and C. Zhou, "Performance study of a fish robot propelled by a flexible caudal fin," in *Proceedings of the 2010 IEEE International Conference on Robotics and Automation*, pp. 90–95, Anchorage, Alaska, USA, 2010.

[4] K. C. Lin, S.-Y. Chen, and J. C. Hung, "Feature selection and parameter optimization of support vector machines based on modified artificial fish swarm algorithms," *Mathematical Problems in Engineering*, vol. 2015, Article ID 604108, 9 pages, 2015.

[5] J. M. Kumph, "The MIT robot pike project [EB/OL]," 2003.

[6] J. Liu and H. Hu, "Mimicry of sharp turning behaviours in a robotic fish," in *Proceedings of the 2005 IEEE International Conference on Robotics and Automation*, pp. 3318–3323, 2005.

[7] M. S. Triantafyllou, A. H. Techet, and F. S. Hover, "Review of experiment work in biomimetic foils," *IEEE Journal of Oceanic Engineering*, vol. 29, no. 3, pp. 585–593, 2004.

[8] X. Tan, M. Carpenter, J. Thon, and F. Alequin-Ramos, "Analytical modeling and experimental studies of robotic fish turning," in *Proceedings of the IEEE International Conference on Robotics and Automation*, pp. 102–108, 2010.

[9] K. H. Low, C. W. Chong, and C. Zhou, "Performance study of a fish robot propelled by a flexible caudal fin," in *Proceedings of the IEEE International Conference on Robotics and Automation*, pp. 90–95, 2010.

[10] R. B. Williams, G. Park, D. J. Inman, and W. K. Wilkie, "An overview of composite actuators with piezoceramic fibers," in *Proceedings of the 20th International Modal Analysis Conference*, pp. 421–427, 2002.

[11] R. B. Williams, D. J. Inman, and W. K. Wilkie, "Nonlinear mechanical behavior of macro fiber composite actuators," in *Proceedings of the Sixth International Conference on Sandwich Structures*, 2003.

[12] R. B. Williams, G. Park, D. J. Inman, and W. K. Wilkie, "An overview of composite actuators with piezoceramic fibers," in *Proceedings of the IMAC XX*, vol. 47, 2002.

[13] https://www.smart-material.com.

[14] A. Ming, K. Hashimoto, W. Zhao, and M. Shimojo, "Fundamental analysis for design and control of soft fish robots using piezoelectric fiber composite," in *Proceedings of the 2013 IEEE International Conference on Mechatronics and Automation*, pp. 219–224, 2013.

[15] W. Zhao, T. Osaka, and A. Ming, "Development of a soft underwater robot mimicking cow-nosed ray," in *Proceedings of the 2011 IEEE International Conference on Robotics and Biomimetics (ROBIO '11)*, 2011.

[16] Z. G. Zhang, N. Yamashita, M. Gondo, A. Yamamoto, and T. Higuchi, "Electrostatically actuated robotic fish: Design and control for high-mobility open-loop swimming," *IEEE Transactions on Robotics*, vol. 24, no. 1, pp. 118–129, 2008.

[17] C. Farhat, M. Lesoinne, and P. LeTallec, "Load and motion transfer algorithms for fluid/structure interaction problems with non-matching discrete interfaces: momentum and energy conservation, optimal discretization and application to aeroelasticity," *Computer Methods in Applied Mechanics and Engineering*, vol. 157, no. 1-2, pp. 95–114, 1998.

[18] J. P. Hung, "Load effect on the vibration characteristics of a stage with rolling guides," *Journal of Mechanical Science and Technology*, vol. 23, no. 1, pp. 89–99, 2009.

[19] I. Harari, K. Grosh, T. J. Hughes et al., "Recent developments in finite element methods for structural acoustics," *Archives of Computational Methods in Engineering*, vol. 3, no. 2-3, pp. 131–309, 1996.

[20] W. Zhao, A. Ming, and M. Shimojo, "Development of high-performance soft robotic fish by numerical coupling analysis," *Applied Bionics and Biomechanics*, vol. 2018, Article ID 5697408, 12 pages, 2018.

[21] Y. Zhang, G. Guan, and X. Pu, "The robot path planning based on improved artificial fish swarm algorithm," *Mathematical Problems in Engineering*, vol. 2016, Article ID 3297585, 11 pages, 2016.

[22] O. C. Zienkiewicz and R. L. Taylor, *The Finite Element Method*, vol. 36, McGraw-hill, London, UK, 1977.

[23] W. Dettmer and D. Perić, "A computational framework for fluid–structure interaction: finite element formulation and applications," *Computer Methods in Applied Mechanics and Engineering*, vol. 195, no. 41-43, pp. 5754–5779, 2006.

[24] J. R. Leach, V. L. Rayz, M. R. K. Mofrad, and D. Saloner, "An efficient two-stage approach for image-based FSI analysis of atherosclerotic arteries," *Biomechanics and Modeling in Mechanobiology*, vol. 9, no. 2, pp. 213–223, 2010.

[25] Q. Gao, Z. Wang, and H. Li, "An optimization algorithm with novel RFA-PSO cooperative evolution: applications to parameter decision of a snake robot," *Mathematical Problems in Engineering*, vol. 2015, Article ID 316826, 12 pages, 2015.

[26] I. Tanaka and M. Nagai, "Hydrodynamic of resistance and propulsion-learn from the fast swimming ability of aquatic animals," *Ship & Ocean Foundation*, pp. 1–219, 1996.